High-throughput discovery of Hf promotion on the formation of hcp Co and Fischer-Tropsch activity

Luis Alvarado Rupflin,[a] Hendrik Van Rensburg,[b] Marco Zanella,[a] Elliot J. Carrington,[a] Alexios Grigoropoulos,[a] Troy D. Manning,[a] John B. Claridge,[a] Alexandros P. Katsoulidis,[a] Robert P. Tooze,[b] and Matthew J. Rosseinsky*[,a]

[a] Department of Chemistry, Materials Innovation Factory, University of Liverpool, Liverpool L7 3NY, U.K.

[b] Drochaid Research Services Ltd, Purdie Building, North Haugh, St Andrews, KY15 9ST

Abstract

A proxy-based high-throughput experimental approach was used to explore the stability and activity of Co-based Fischer Tropsch Synthesis catalysts with different promoters on various supports. The protocol is based on the estimation by XRD of active phase, Co, particle size and relative amounts of crystalline phases, Co to support. Sequential libraries samples enabled exploration of four Co loadings with five different promoters on six support materials. Catalysts stable to aging in syngas, displaying minimal change of particle size or relative area, were evaluated for their activity under industrial conditions. This procedure identified SiC as support for stable catalysts and a combination of Ru and Hf to promote the formation hcp Co. Unsupported bulk samples of Co with appropriate amounts of Ru and Hf revealed that the formation of hcp Co is independent of the support. The hcp Co containing catalyst presented the highest catalytic activity and C_{5+} selectivity amongst the samples tested in this study confirming the effectiveness of the proxy-based high-throughput method.

Introduction

The Fischer Tropsch Synthesis (FTS) is an important process for the production of long chain hydrocarbons from syngas (a mixture of CO and H_2) using Co and Fe based catalyst materials. The development of active and stable catalysts for FTS is particularly difficult due to the complex nature of the reaction and the complex interactions between active material, support and promotors, the mixture of similar products and the long-time experiments needed for the measurement of activity and stability [1-3]. The activity of FTS catalysts is attributed to different factors such as the particle size, active metal phase, the metal surface area, and the interactions with the support material [4-7]. The presence of different Co polymorphs (fcc and hcp) for example plays an important role in the activity of the catalysts and has been subject to many studies recently, showing that the hcp Co phase is more active than the fcc Co phase in FTS [1, 2, 8-10]. The deactivation of the catalysts can occur through different mechanisms like sintering, oxidation, formation of metal-support compounds, carbon deposition and poisoning [4, 7, 11, 12]. Realistic investigations addressing the activity and stability of FTS catalysts require extended testing times and diverse catalyst sets to delineate the effect of the different factors.

The formation and stabilization of the hcp Co phase for FTS catalysts has been thoroughly investigated [1, 2, 8-10, 13, 14]. The hcp Co phase is destabilized with increasing temperature because of its higher

surface energy compared to fcc Co [15]. Thus, above a temperature of approx. 400 °C fcc Co is the main phase observed [16]. de la Pena et al. [17] reported the formation of Co hcp particles by reducing Co_3O_4 nanoparticles in a H_2 and CO gas mixture. The authors observed the formation of a graphitic layer encapsulating the hcp Co particles, which stabilizes the hcp phase by decreasing the surface energy and inhibits the phase change. Under these conditions the hcp Co phase remains stable up to a temperature of 700 °C. To achieve the formation of the hcp phase on a support material, Gnanamani et al. [2] treat supported Co samples under CO flow and moderate temperatures (230 °C) to form the Co carbide (Co_2C). The reduction of the Co_2C at 230 °C under H_2 leads to the formation of the hcp Co phase. The enhancement of the formation of the hcp Co from Co_2C is attributed to structural similarity between these phases as both crystallize in the hexagonal system. Unfortunately, the samples were not reduced at temperatures higher than 230 °C to observe if the Co hcp phase remains stable. No investigation has, to our knowledge, facilitated the formation of the Co hcp phase by adding promotors and reducing the samples under H_2 at temperatures as high as 500 °C.

High throughput (HT) experimentation is used to accelerate the screening of large catalyst sets, it has been successfully applied in the development of heterogeneous catalysts [18-20], and can be applied for the identification of stable FTS catalysts, by parallelizing the preparation, ageing and characterization of the samples. While testing the catalytic properties of the materials demands access to expensive and specialised equipment [21], the use of a proxy can accelerate the identification of suitable, stable and active materials without having to test all of them. In a previous paper [5] we reported the development of a proxy based method for the accelerated discovery of stable FTS catalysts. The workflow (Figure S1) developed includes the parallelized preparation, reduction, characterization of the samples augmented by an aging procedure under FTS similar conditions (H_2:CO = 3; 230 ºC, 1 bar) for 100 h. The core of the proxy is the assessment of the stability and activity of the samples by estimating the change in particle size and the amount of metallic Co with the aging procedure. This is carried out by comparing the Co peak width and area (calculated relative to the support peak area). The last step is to run rapid high throughput TGA on selected samples to estimate the degree of reduction. The use of this method identified the composition of a series of highly stable, high surface area supported Co catalysts promoted by Mg and Ru, and the optimization of the preparation protocol (i.e. order of addition, calcination steps).

The proxy described above is applied herein to investigate the effect of different support materials and promotors on the stability of Co based catalysts. The iterative workflow was used to first screen six different support materials (active carbon, Al_2O_3, SiC, SiO_2, TiO_2, ZrO_2) and five promotors (Ru, Re, Mo, Mn, La). This set of experiments identified SiC as a suitable support material and the screening of further promotors (Ru, La, Ce, Pr, Nd, Hf) lead to the identification of the positive effects of a combination of Co, Ru, Hf on SiC, which shows the formation of hcp Co phase under our standard reduction conditions. Catalytic experiments under real FTS conditions revealed higher C_{5+} selectivity for a catalyst promoted with Ru and Hf. A more comprehensive study of the effects of Ru and Hf on the formation and stabilization of the hcp Co phase without support materials, shows that Ru and Hf alone stabilize this phase, but the effect increases significantly, when both are present, stabilizing the hcp Co phase to a temperature up to 500 ºC and 12 h.

Experimental

Sample preparation

Catalysts were synthesized by incipient wetness impregnation of the support materials. The support materials were weighed by a Quantos automated balance (Mettler Toledo XPE206) (250 mg) into 24 vials. An Eppendorf ep Motion 5075 was used for the liquid deposition onto the support materials; a

plate holding an array of 4 x 6 vials containing the weighed support materials, allowed a variation of four different Co loadings and five different promotors on each support material (six support materials), this gives a total of 24 samples with different composition on each of the six support materials, *i.e.,* a total of 144 samples.

The impregnation of the support materials is a multistep procedure. In a typical synthesis of a material with 20 wt.-% of Co, 0.212 ml of a 4.0 M $Co(NO_3)_2 \cdot 6H_2O$ solution were added to the 24 vials each containing 250 mg of SiC using the Eppendorf ep Motion 5075, followed by the addition of 0.047 ml of water. After mixing the materials with a spatula, the vials are placed on a shaker for 1 h to obtain a homogenous distribution of the solution on the support material. The samples were dried at 100 °C for 16 h. The impregnation of each promoter (Ru, Re, Mo, Mn, La, Ce, Pr, Nd and Hf) is performed with the respective solution and water amounts, followed by a final drying step at 100 °C for 16 h and subsequent heat treatment at 300 °C under air for 6 h for the decomposition of the nitrates. The exact amount of promotor precursors and solutions used in each impregnation are provided in the Supporting Information file. The following step is the reduction of the samples under pure hydrogen flow (50 ml/min) at 500 °C for 12 h in ceramic well plates (128x43x6 mm, Figure S2). The ceramic well plate can hold 48 different samples and three of the plates can be reduced each time, making a total of 144 samples per run. Before taking the catalysts out of the furnace they are passivated with 1 % O_2 in N_2 (100 ml/min) at room temperature. The ceramic well plates are directly placed in a high throughput XRD (HT XRD, Panalytical X-pert Pro diffractometer with an XYZ stage) for the first characterization of the samples. The ceramic well plates are designed to fit on the XYZ stage.

The aging procedure of the samples was performed using the ceramic well plates under conditions approximating low temperature FTS with the flow of syngas (H_2:CO = 2:1, 90 ml/min) at 230 °C and ambient pressure for 100 h. After the aging procedure the samples are passivated and transferred to the HT XRD for characterization.

Scale up of samples

Samples selected for scale up were prepared manually in an identical manner to the procedure described above. In a typical synthesis, a sample with 20 wt.-% Co, 0.1 wt.-% Ru, and 5 wt.-% Hf supported on SiC (CoRuHf SiC) was prepared as follows: 1.697 ml of the 4.0 M $Co(NO_3)_2 \cdot 6H_2O$ solution was added to 0.463 ml water and deposited on 2 g of SiC in a porcelain dish (80 mm diameter) placed on a shaker. The sample was dried at 100 °C for 16 h, prior to the next impregnation. The next impregnation with the 0.1 M $Ru(NO)(NO_3)_3$ solution is performed in an identical manner, but with the respective solution (0.197 ml) and water (2.083 ml) amounts, followed by a drying step at 100 °C for 16 h. Finally, the impregnation with 0.47 M $HfCl_2O$ is performed with the respective solution (1.192 ml) and water (0.974 ml) amounts, followed by a last drying step at 100 °C for 16 h and a posterior heat treatment at 300 °C under air for 6 h for the decomposition of the nitrates. The second step is the reduction of the samples, which was performed in a tube furnace under pure hydrogen flow (50 ml/min) at 500 °C for 12 h in ceramic boats (80 mm). Before taking the catalysts out of the furnace they are passivated at room temperature with 1 % O_2 in N_2 (100 ml/min).

Unsupported samples

Unsupported samples were prepared by mixing quantities of the solutions to obtain the desired atomic ratios. In a typical synthesis of a sample with Ru:Co = 0.003 and Hf:Co = 0.08 atomic ratios 1.073 ml of the 4 M $Co(NO_3)_2 \cdot 6H_2O$ solution, 0.127 ml of the 0.1 M $Ru(NO)(NO_3)_3$ solution and 0.722 ml of the 0.47 M $HfCl_2O$ solution were mixed together. After mixing the solutions, the drying, calcination and reduction steps are identical as for the supported samples described above.

Characterization

High-throughput X-ray diffraction, XRD, was performed on a Panalytical X-pert Pro diffractometer with an XYZ stage using Co $K\alpha_1/\alpha_2$ (ratio = 2) radiation between 38°-55° 2θ, with a 0.039° step size and 283 s/step. The particle size of the Co metal phase was calculated from the line broadening of the most intense fcc Co peak (111) using the Scherrer equation in X'Pert HighScore Plus software using a Si standard to determine the instrumental line width. Relative crystallinity was determined from the Co (111) to support XRD peak area ratio.

XRD of bulk samples was performed with a Panalytical X-pert Pro in Bragg-Brentano geometry laboratory X-ray diffractometer with Co K_{a1} radiation = 1.78901 Å. Synchrotron XRD data was recorded on beamline I11 (λ = 0.825972 Å) at Diamond Light Source, UK.

Temperature programmed reduction (TPR) was measured using a Quantachrome ChemBET 3000 unit with a TPD; ca. 50 mg of the calcined sample were loaded into a quartz cell and heated up to 100 °C for 30 min under He (100 ml/min) to remove moisture and other adsorbed species from the samples. After cooling down to room temperature the sample was heated to 750 °C at 5 °C min^{-1} under a flow of 5% H_2 in N_2 (100 cm^3 min^{-1}) to perform the analysis.

Fischer -Tropsch Synthesis

The activity tests in the FTS were performed at Drochaid Research Services Ltd in St. Andrews. The high throughput catalyst testing was done using a custom-built 32-tube fixed bed reactor test plant, designed by Integrated Lab Solutions and built by Premex. One unit, consisting of two heating blocks with eight reactors each, was used for the tests. The reactors (L = 300 mm; ID = 2.4 mm; OD = 6.5 mm) were accommodated in a heating furnace with an isothermal zone of 100 mm. The catalyst bed length is of 7 cm with in the isothermal zone. SiC was used as an inert diluent material. The flow of the gases CO (CP grade, BOC), H_2 (CP grade, BOC) and Ar (CP grade, BOC) as an internal standard was controlled by mass flow controller and the pressure by a digital back pressure regulator. The concentration of reaction educts and products was measured using online GC techniques (Agilent Refinery Gas Analyser with a FID channel for the quantification of light hydrocarbons (DB-1 column (2m x 0.32mm x 5µm) and HP-AL/S column (25m x 0.32mm x 8 µm)) and two TCD channels; TCD1 for the permanent gases CH_4, CO_2, Ar, N_2, and CO (HayeSep Q column (6 ft., 80/100 mesh) and a Mol Sieve 5A column (6 ft., 60/80 mesh)) and TCD2 for H_2 (HayeSep 3 ft.,80/100 mesh and Molsieve 8 ft., 60/80 mesh).

Results and Discussion

Results of the first library

The HT exploration of FTS catalysts is based on the prior assessment of stability of the active phase, metallic Co, on treatment with syngas as proxy for their activity. The applied workflow involves the parallel synthesis, syngas treatment and XRD characterisation of sample libraries. These are prepared by automated incipient wetness impregnation and reduced concurrently by H_2 at 500 ºC. HT-XRD analysis is employed to determine the phase of Co and its particle size before and after the aging of samples under a syngas mixture, H_2:CO = 2:1, at 230 ºC for 100 h. Large changes in the particle size of Co or in its overall crystallinity, estimated by the peak area ratio of Co to support, are taken as indicators of the lack of stability and predictors of low activity catalyst in FTS.

The effects of the support material, the Co loading and the addition of promotors were investigated in the first library, which consisted of 144 samples. Support materials Al_2O_3 [1, 11, 22-30], TiO_2 [6, 11, 28, 31-37] ZrO_2 [28, 32, 33], SiO_2 [2, 11, 28, 32, 38-45] active carbon (AC) [27, 30, 46, 47], and SiC [48, 49] were used. Despite the reactivity of metal oxides, particularly Al_2O_3, with Co they were selected as supports for their porosity and thermal stability. Non-oxide supports do not interfere with Co, which can be reduced at relatively low temperatures. Ru, Re, Mo, Mn and La were used as promotors. Ru and Re known to increase the reducibility of cobalt on support materials [6, 11, 25, 26, 28, 31, 33] and increase the resistance to deactivation. Furthermore Ru is known to be the most active element in FTS. The transition metals Mo and Mn were selected too, since they have been reported to increase the chain-growth probability factor to larger hydrocarbons in the product stream [30, 35, 40, 44, 45, 50, 51] and finally the rare earth metal La, which has been reported to increase the dispersion of Co on the support [28, 29, 37, 42, 44, 46, 52].

Table 1 Overview of the of the first library with 144 different compositions (support x Co loading x promoter): six different support materials with four different Co loadings each and six different promotors (none, Ru and Re with low loading levels (0.1 wt.-%) and Mo, Mn and La with high loading levels (5.0 wt.-%))

Support	Co loading (%)	Promoter
Al_2O_3	5	-
SiO_2	10	Ru (0.1%)
TiO_2		Re (0.1%)
ZrO_2	15	Mo (5%)
SiC	20	Mn (5%)
AC		La (5%)

Based on a first assessment of the HT XRD patterns, samples showing no metallic Co peaks after the reduction or after the aging procedure were immediately ruled out. This is the case for the samples supported on ZrO_2 and samples with only 5 wt.-% Co loading on every other support. The results of crystallite size analysis for aged samples are plotted versus the crystallite size before aging (Fig. 1a). The y=x line is used to display the increase, points above the line, or the decrease, points below the line, of the crystallite size after the syngas aging process. Samples prepared on SiO_2, AC and TiO_2 show an increase in the crystallite size after aging, up to a doubling of the particle size after the aging procedure observed for SiO_2, AC and TiO_2, while the samples supported on SiC show an increase to a lesser extent, from 27 to 36 nm. For samples supported on Al_2O_3 a decrease of the particle size from 33 to 16 nm, in the most extreme case, was observed. Figure 1b shows the peak area ratio between Co and support, for the three crystalline supports (Al_2O_3, TiO_2 and SiC), before and after the aging procedure. TiO_2 and Al_2O_3 show a decrease of the peak area ratio after the aging procedure (up to 70 % Co peak area ratio loss on samples supported on TiO_2 and up to 60 % Co peak area ratio loss on samples supported on Al_2O_3), while the area ratio of samples on SiC show the smallest change (between 8 and 23 % Co peak area ratio increase). The effect of the different promotors can clearly be observed for the samples supported on SiC (Figure 1c and d). The samples that show the smallest change in the Co peak area ratio, are those promoted with Ru (from 0.63 to 0.75), La (from 0.65 to 0.83) and Mo (from 0.70 to 0.77).

Since samples prepared on SiC show the smallest change of Co crystallite size and peak area ratio after the aging procedure, they were identified as hits from the first library. The samples with a Co loading of 15 wt.-%; promoted with Ru and Re, at 0.1 wt.-% loading, and Mn, Mo or La, 5 wt.-% loading were scaled up and tested in FTS under industrial conditions. These samples were named after the active component and the promoter, *i.e.* the sample CoRu had 15 wt.-% Co and 0.1 wt.-% Ru. The cobalt time yield of each sample on FTS at 20 bar and three different temperatures is shown on Figure 2. At all three

temperatures the sample CoRuLa showed the highest activity, CoMn showed the lowest and the other five samples Co, CoRu, CoRe, CoLa and CoMo showed similarly intermediate activity. Apart from the highest activity the sample CoRuLa also exhibited the highest selectivity for liquid products, C_{5+} 80.75%, and very low selectivity towards CO_2 (Table 2). Promotors Ru and Re did not enhance the selectivity of C_{5+} compared to Co sample while CoMn, CoMo and CoLa provided significantly lower C_{5+} selectivities.

The positive effect of the simultaneous promotion of Ru and La on the activity of the catalyst prompted the further investigation of similar systems, in this case expanding the investigation of the promotion with other rare earth metals, which will be discussed in the next section.

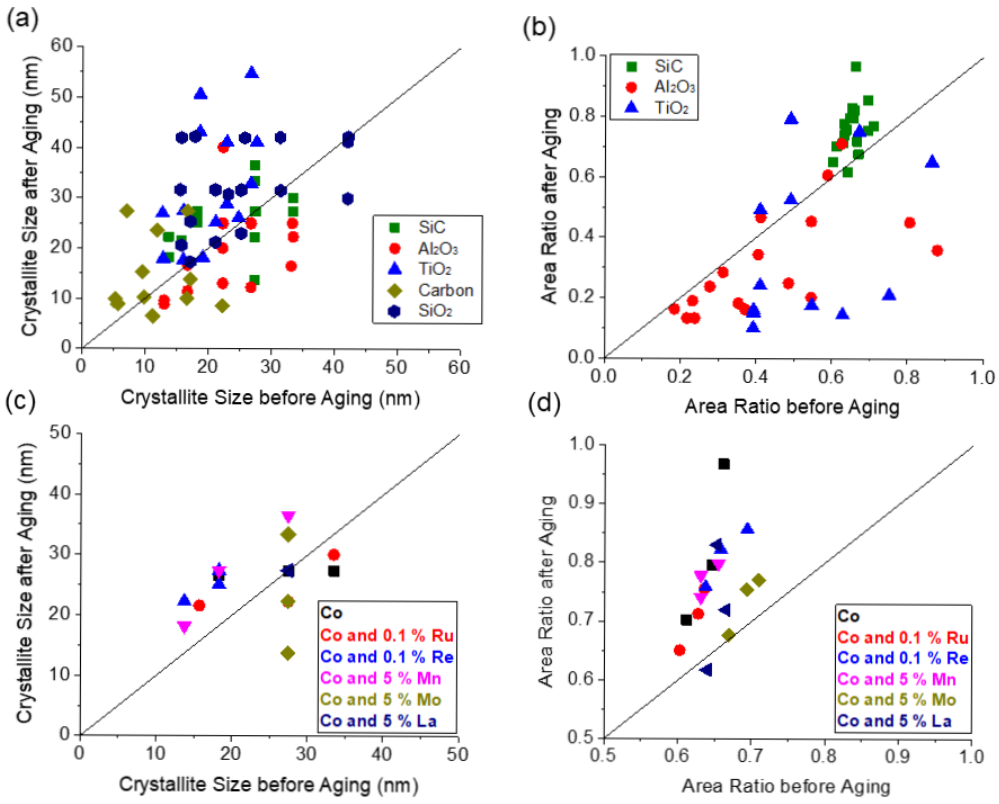

Figure 1 HT screening of the first library. (a) The effect of the support material on the changes of Co crystallite size and (b) peak area ratio with syngas aging. (c) The effect of promoter on the changes of Co crystallite size and (d) peak area ratio of SiC supported samples with syngas aging.

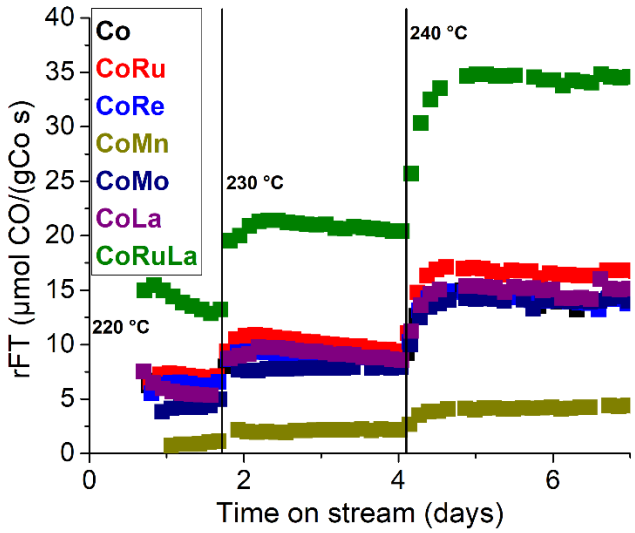

Figure 2 The cobalt time yield on FTS of seven catalysts with different promotors at three different temperatures.

Table 2. FTS rate and gas phase product distribution at 230 °C of the catalysts with different promotors.

Sample		Temperature	Selectivity				FTS Rate
Composition	Support	°C	CH_4 %	C_{2-4} %	C_{5+} %	CO_2 %	[µmol CO/(gCo s)]
Co	SiC	230	11.22	10.93	76.46	1.39	9.06
CoRu	SiC	230	9.33	9.83	78.55	2.28	10.07
CoRe	SiC	230	10.85	11.74	76.10	1.31	9.02
CoMn	SiC	230	26.17	29.64	44.19	0.00	2.17
CoMo	SiC	230	15.99	13.59	65.90	4.52	7.86
CoLa	SiC	230	10.55	16.23	72.60	0.62	9.25
CoRuLa	SiC	230	8.74	10.06	80.75	0.44	20.69

Results of the second library

A second library focussed on the effect of the content of Ru and the inclusion of rare earth elements (La, Ce, Pr, Nd), and Hf as promotors for Co-based materials supported on SiC. The proxy screening on the first library proved the suitability of SiC as a support material and the positive effect of Ru and La on the stability of Co after the aging procedure. Furthermore, the first catalytic test showed the positive effects of the simultaneous promotion of La and Ru enhancing the CO conversion rate and the C_{5+} selectivity.

While the effect of rare earths on Co-based catalysts has been thoroughly investigated [44, 45, 52, 53], little is known about the effect of the promotion of Hf [34] and its effect on the phase formation and stabilization of Co particles. Hf was chosen, because it is in the same group as Ti and Zr, whose oxides are known promotors and support materials for FT catalysts and because it is in the same period as the rare earth metals. Many patents mention the use of Hf as a promoter for Co based FTS catalysts, but only one patent [34] could be found, where experimental data showing the positive effect of Hf promotion of Co based catalysts is presented.

The effect of rare earths (La, Ce, Pr, Nd) or Hf addition at different loading levels was investigated for samples loaded with Co and Co and Ru, as shown in Table 3. The results obtained after submitting the samples to the workflow described above can be seen in Figure 3, where peak area ratio of Co after the aging procedure is plotted over the peak area ratio before the aging procedure. Each colour represents a different promoter, the shape of the symbols represents different levels of each promoter and the open symbols represent samples without Ru. Samples with Ru and 2.5 or 5 wt.% Hf, along with samples promoted with Ru and Ce and samples with Ru and Pr, show a good stability under aging conditions. Samples promoted without Ru prove to be stable under the aging conditions but show lower Co peak area ratios than samples promoted with Ru. The samples promoted with Ru and Hf are particularly striking, whilst the sample with 5 wt.% Hf and 0.1 wt.% Ru stabilizes the Co peak area as shown in Figure 3, it also shows a further peak on the XRD patterns, which corresponds to the hcp Co phase (Figure S3 SI). The formation of the hcp phase can only be observed for samples promoted with Hf and Ru.

Table 3 Overview of the 30 different compositions of the second library prepared on SiC, combining the promotion of Co catalyst with Ru and rare earths or Hf.

Co and Ru (wt%)		**Promoter** (wt%)							
		RE (La, Ce, Pr, Nd)				Hf			
20	-	-	5	10	-	-	2.5	5	-
20	0.1	2.5	5	10	15	1.25	2.5	5	10

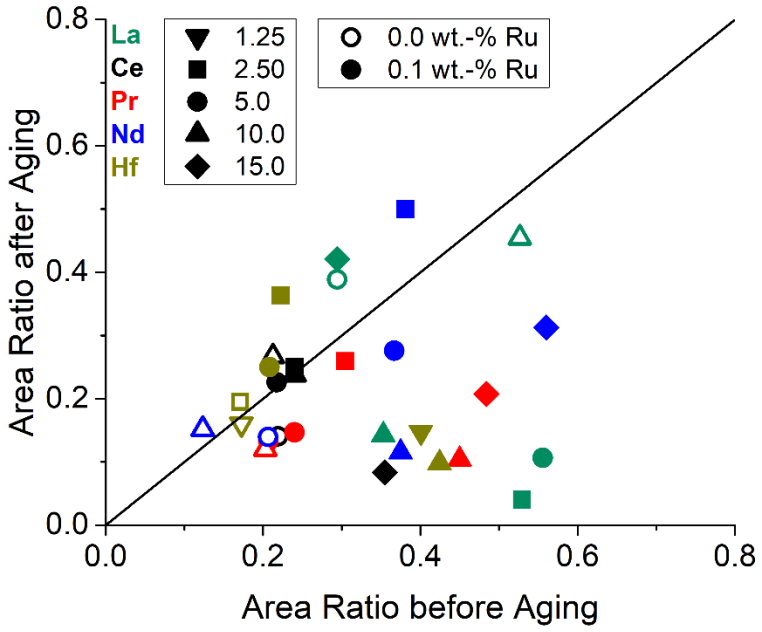

Figure 3 Results of the proxy evaluation of the effect of the addition of La, Ce, Pr, Nd, Hf and Ru to Co based samples supported on SiC

Scale up of samples

The samples with 5 wt.% loading of promotors displayed the highest stability in the proxy screening of the second library and they were selected for scale up, characterisation and FTS testing. All samples have fixed loadings of Co (20 wt.%), Ru, (0.1 wt.%), and either Ce, Pr, La or Hf (5 wt.%) or no promoter.

A sixth sample with standard Co loading (20 wt.%) alone supported on SiC was made for comparison purposes. The samples are named according to the active component and the promotors in a similar fashion to the first set of samples.

The XRD patterns of the six scaled up samples and of the pure SiC obtained from the synchrotron source at Beamline I11 of Diamond Light Source are presented in Figure 4. The catalysts show the formation of the fcc Co phase, displaying peaks at d-spacing of 2.04 and 1.77 Å (the (111) and (200) lattice planes respectively). The sample promoted with Hf displays further peaks at d-spacing of 1.91 and 1.15 Å that correspond to the hcp phase of Co (the (101) and (110) planes respectively). The catalysts promoted with Ru, Ce and Ru, and Pr and Ru also show small and broad peaks at a d-spacing of 1.91 but with a very low intensity. A strong enhancement of the formation of the hcp Co phase can only be observed in the sample promoted with Hf and Ru.

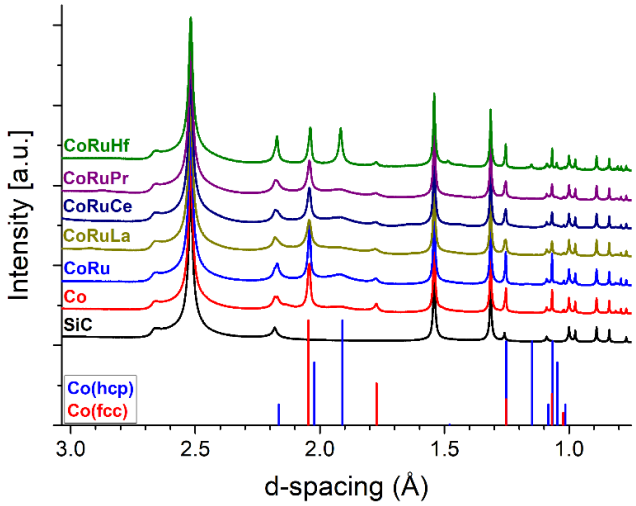

Figure 4 Synchrotron PXRD patterns of the six scaled up samples selected from the second library and of the pure SiC.

Temperature programmed reduction

In order to understand the effect of each promoter on the reduction behaviour of Co, the samples were submitted to a TPR analysis under 5 % H_2 in N_2 (Figure 5). The sample containing only 20 wt.-% Co shows two different peaks, the first at a lower temperature (300-375 °C) is associated with the reduction of the Co(III) species to Co(II), and the second one, at a higher temperature (400-500 °C) with the reduction of the Co(II) species to Co(0) [28]. The addition of Ru to the samples enhances the reducibility of the samples lowering the temperature of both reduction steps. The addition of both Ru and rare earth metals as promotors leads to an increase of the reduction temperature for both steps, compared to those promoted by Ru alone, as illustrated by the TPR for the samples promoted with Ru and La or Pr. The sample promoted with mixture of Ru and Ce shows similar reduction behaviour in relation to the sample promoted only with Ru. Again it is the sample promoted with Ru and Hf which shows the most differentiated reduction behaviour. The reduction temperature of the Co(III) species is raised to ca. 350 °C, simultaneously the reduction temperature for the Co(II) species is reduced to ca. 400-450 °C. The peaks for both steps merge together in a single reduction peak between 325-450 °C, where they cannot be differentiated from each other.

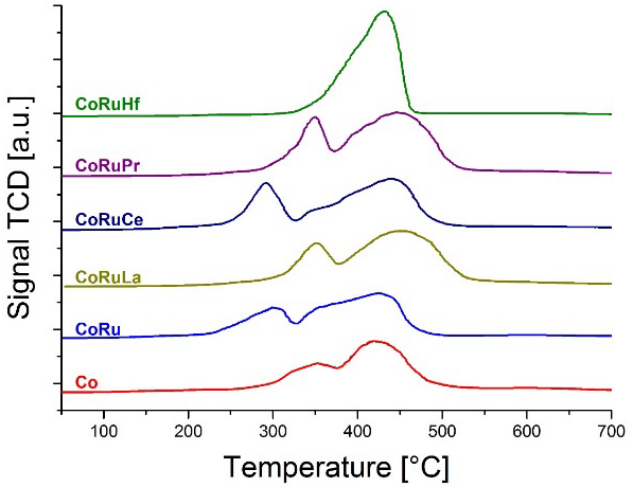

Figure 5 H_2-TPR profile of the scaled-up samples. The addition of Hf to the samples leads to a merge of the reduction peaks of Co oxides.

Fischer-Tropsch Synthesis

The scaled-up materials were tested under industrial FTS conditions in a parallel reactor system at 20 bar and three different temperatures (Figure 6a). At 210 ºC the materials CoRu, CoRuLa, CoRuCe and CoRuPr show similar Co time yield and only the material CoRuHf shows higher performance. At 220 °C all the materials display an increase in their activity with CoRuHf being the most active and CoRuPr showing higher yield than the rest of the samples. At 230 °C all the materials show different CO conversion rates in the FTS with the following activity order CoRuHf> CoRuPr> CoRuLa> CoRuCe> CoRu. The material promoted with Ru and Hf not only shows the highest yield at all temperatures, it also displays the highest selectivity values towards C_{5+} components as Table 4 shows. The material CoRuHf achieves C_{5+} selectivity values up to 80.19 % with a CO conversion rate of up to 23.90 µmolCO/(gCo·s), followed by the CoRuCe material (77.33 % C_{5+} selectivity and 20.22 µmolCO/(gCo·s)), the CoRu material, which shows high selectivity towards C_{5+} components (76.90 %) but lower CO conversion rates (14.43 µmolCO/(gCo·s), and the CoRuPr material (75.38 % C_{5+} selectivity and 20.38 µmolCO/(gCo·s)). The material with the lowest C_{5+} selectivity is CoRuLa with 68.57 % and 17.14 µmolCO/(gCo·s). Furthermore, the CoRuHf material also shows the lowest selectivity towards CO_2 (0.36 %) and C_2-C_4 components (7.90 %) at 230 ºC. Finally, the CoRuHf material shows a selectivity towards CH_4 of 11.55 % at 230 °C, which is only lower than the selectivity achieved by the CoRuLa material (11.84 %). Methane, being a raw material for the production of syngas, and CO_2, are undesired by-products in FTS [54].

A comparison between the fresh and used samples is shown on Figure 6b. Compared with the fresh catalysts the XRD characterization of the spent catalysts shows no significant loss of the fcc Co phase for any of the catalysts. The CoRuHf shows the presence of the hcp Co phase in the fresh and in the spent material. Both fcc and hcp Co phases are stable under the testing conditions, *i.e.,* the deactivation observed at 230 ºC during the catalytic test is not caused by the formation of Co oxides.

The higher yield and the higher C_{5+} selectivity values of the Hf containing material compared to the rest of the catalysts is consistent with the formation of the hcp Co phase. The effect of the formation of the different phases on the activity of the catalysts has been studied previously [1-3, 9, 10, 23, 41]. By treating the materials under different conditions, phase pure fcc and hcp Co catalysts were prepared on the support materials, as investigations by Lyu [10] and Gnamani [2] showed. The comparison between the activities of those materials demonstrated that catalysts with the hcp phase achieved a higher activity

than the other materials. DFT calculations indicate that hcp Co has a higher activity for CO activation in the presence of H_2 than fcc Co [9].

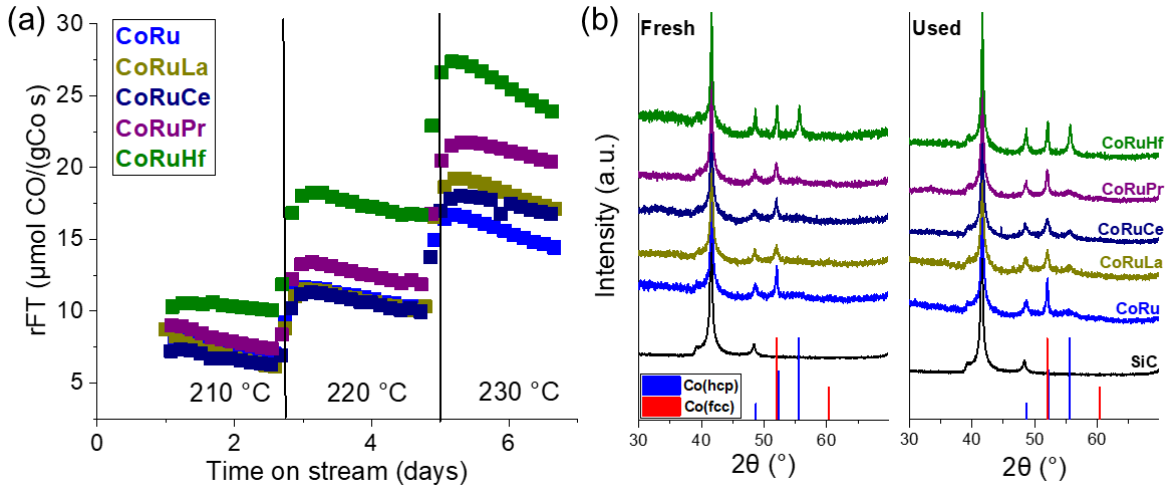

Figure 6 (a) Cobalt time yield on FTS from the catalysts selected from the second library. (b) Comparison of the fresh and spent catalyst materials.

Table 4 FTS rate and products' selectivity at 230°C of the catalysts selected from the second library.

Sample Composition	Support	Temperature °C	Selectivity CH_4 %	C_{2-4} %	C_{5+} %	CO_2 %	FTS Rate [µmol CO/(gCo s)]
CoRu	SiC	230	11.48	10.80	76.90	0.82	14.43
CoRuLa	SiC	230	11.84	18.99	68.57	0.60	17.14
CoRuCe	SiC	230	9.48	12.64	77.33	0.55	20.22
CoRuPr	SiC	230	10.14	14.00	75.38	0.48	20.38
CoRuHf	SiC	230	11.55	7.90	80.19	0.36	23.90

Unsupported Samples

The formation of the hcp Co phase supported on SiC and promoted with Hf and Ru motivated us to further investigate the effect of Hf and Ru on formation of hcp Co. To eliminate the effect from the support material a set of samples with different Hf:Co and Ru:Co atomic ratios were prepared and reduced at different temperatures and for different times. Samples showing a reduction time of 0 h were held at the reduction temperature for 5 min before cooling down at a natural rate. The results from the XRD characterization (Fig. 7) show the patterns of samples with three different Hf:Co ratios reduced at different temperatures and for different times. The sample with Hf:Co = 0 is reduced completely at 300 °C and shows the formation of the hcp Co phase. An increase in the reduction temperature leads to the formation of the fcc Co phase. The formation of the fcc phase can be observed by the increase of intensity of the (111) peak (2θ = 52.01°). At a reduction temperature of 500 °C almost all the hcp Co has been converted to fcc phase. The (200) peak (2θ = 60.34°) of the fcc Co phase can be observed clearly while there is an associated significant decrease in intensity of the (100) and (101) peaks of the Co hcp phase. The phase composition of each sample has been obtained by Rietveld refinement (Figure S4). The decrease in the content of the hcp Co phase proceeds with longer reduction times, but even

after 12 h at 500 ºC, the content of hcp Co phase is 45 wt%. The addition of Hf to the sample impedes the reduction of the samples and the conversion of the hcp into the fcc Co phase, as the XRD patterns of the samples with Hf:Co = 0.04 and Hf:Co = 0.08 show. Samples with Hf:Co = 0.04 reduced at 300 ºC show mainly the peaks of CoO and some hcp Co. An increase in temperature to 350 ºC leads to further formation of the hcp Co. At 400 ºC only the mettalic Co phases can be observed, while increasing the temperature to 500 ºC and reduction times at 12 h hcp Co remains the dominant phase, 84 wt%. The behaviour of the samples with Hf:Co = 0.04 and Hf:Co = 0.08 is very similar. At 300 ºC only CoO is present in the sample, and at 400 ºC the most of the CoO has been transformed to the metallic hcp Co phase. Reducing the sample at 500 ºC for 12 h the most of Co is present as the hcp phase, 86 wt% while very broad peaks corresponding to monoclinic HfO_2 have been appeared.

The addition of Ru to the sample promotes the formation of the hcp Co phase at low temperature as no oxide phase is detected in any of the samples (Figure 8a). The content of hcp phase is higher, at all reduction temperatures, when compared to the samples with no Ru (Figures S4 and S5). The stabilization of the hcp Co phase is enhanced when the samples are promoted with Ru and Hf as shown by the XRD patterns in Figure 8 b and c. The samples with Ru:Co = 0.003 and Hf:Co = 0.04 or Hf:Co = 0.08 indicate that even after 12 h reduction time at 500 ºC the content fcc Co phase reaches only 6 wt% and 11 wt% respectively.

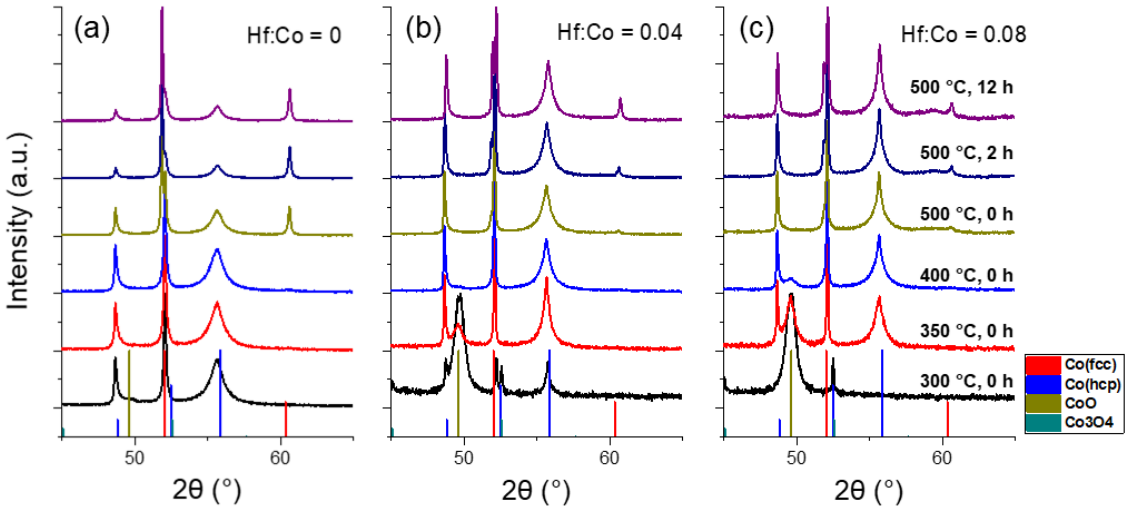

Figure 7 PXRD patterns of unsupported Co samples with (a) Hf:Co = 0, (b) Hf:Co = 0.04 and (c) Hf:Co = 0.08 and reduced at different temperatures and times.

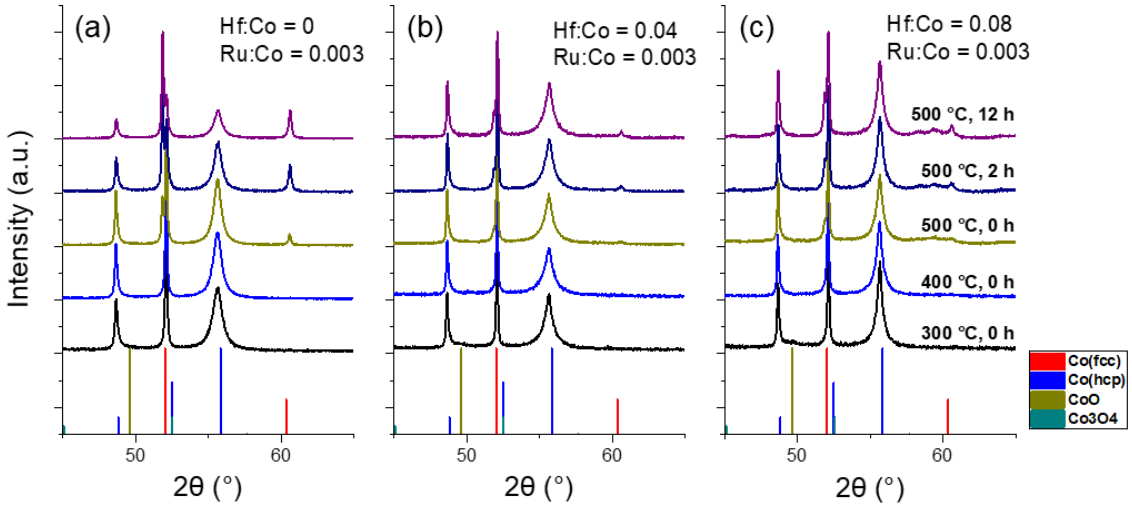

Figure 8 PXRD patterns of unsupported Co samples with Ru:Co = 0.003 and with (a) Hf:Co = 0, (b) Hf:Co = 0.04 and (c) Hf:Co = 0.08 and reduced at different temperatures and times.

Conclusions

Applying the described high throughput protocol we were able to screen different support materials and promotors for the Co based FTS catalysts. The protocol allowed us to identify SiC as a suitable support for active and stable catalyst materials. Furthermore the promotors Ru and Hf were identified, to not only increase the stability of the materials, but also to enhance the formation of the hcp Co phase, which is known to be more active in FTS than the fcc Co phase.

Samples containing Co, Ru and Hf were scaled up alongside other samples promoted with Ru and rare earth elements and tested in the FTS under industrial conditions (230 ºC, 20 bar). Here the material with Co, Ru and Hf showed higher CO conversion than the other materials tested and also showed the highest selectivity values towards C_{5+} components. The higher conversion and selectivity of this materials is attributed to the formation of the hcp Co phase.

The further investigation of the effect of Hf in the formation of the different phases of Co shows that Hf shifts the reduction of CoO to higher temperatures and stabilizes the hcp phase at higher temperatures (500 °C) also during longer reduction times. The addition of Ru to the samples facilitates the reduction of CoO, such that all samples, even samples with higher amounts of Hf (up to 0.08 molar ratio) are reduced at temperatures of 300 ºC. The simultaneous addition of Ru and Hf to the samples inhibits the transformation of the hcp to the fcc phase, to a greater extent than achieved by the addition of Hf only.

Acknowledgements

This work was supported by the Engineering and Physical Sciences Research Council (EPSRC), UK (EP/N010531/1). We thank the Diamond Light Source for provision of beam time on the I11 beamline. M.J.R. thanks the Royal Society for the award of a Research Professorship.

References

[1] J.-S. Jung, J.-S. Lee, G. Choi, S. Ramesh, D.J. Moon, The characterization of micro-structure of cobalt on γ-Al_2O_3 for FTS: Effects of pretreatment on Ru–Co/γ-Al_2O_3, Fuel, 149 (2015) 118-129.
[2] M.K. Gnanamani, G. Jacobs, W.D. Shafer, B.H. Davis, Fischer–Tropsch synthesis: Activity of metallic phases of cobalt supported on silica, Catalysis Today, 215 (2013) 13-17.
[3] A.Y. Khodakov, Fischer-Tropsch synthesis: Relations between structure of cobalt catalysts and their catalytic performance, Catalysis Today, 144 (2009) 251-257.
[4] M. Argyle, C. Bartholomew, Heterogeneous Catalyst Deactivation and Regeneration: A Review, Catalysts, 5 (2015) 145.
[5] P. Boldrin, J.R. Gallagher, G.B. Combes, D.I. Enache, D. James, P.R. Ellis, G. Kelly, J.B. Claridge, M.J. Rosseinsky, Proxy-based accelerated discovery of Fischer-Tropsch catalysts, Chemical Science, 6 (2015) 935-944.
[6] J. Li, G. Jacobs, T. Das, B.H. Davis, Fischer–Tropsch synthesis: effect of water on the catalytic properties of a ruthenium promoted Co/TiO_2 catalyst, Applied Catalysis A: General, 233 (2002) 255-262.
[7] D.J. Moodley, J. van de Loosdrecht, A.M. Saib, M.J. Overett, A.K. Datye, J.W. Niemantsverdriet, Carbon deposition as a deactivation mechanism of cobalt-based Fischer–Tropsch synthesis catalysts under realistic conditions, Applied Catalysis A: General, 354 (2009) 102-110.
[8] L. Braconnier, E. Landrivon, I. Clémençon, C. Legens, F. Diehl, Y. Schuurman, How does activation affect the cobalt crystallographic structure? An in situ XRD and magnetic study, Catalysis Today, 215 (2013) 18-23.
[9] J.-X. Liu, H.-Y. Su, D.-P. Sun, B.-Y. Zhang, W.-X. Li, Crystallographic Dependence of CO Activation on Cobalt Catalysts: HCP versus FCC, Journal of the American Chemical Society, 135 (2013) 16284-16287.
[10] S. Lyu, L. Wang, J. Zhang, C. Liu, J. Sun, B. Peng, Y. Wang, K.G. Rappé, Y. Zhang, J. Li, L. Nie, Role of Active Phase in Fischer–Tropsch Synthesis: Experimental Evidence of CO Activation over Single-Phase Cobalt Catalysts, ACS Catalysis, (2018) 7787-7798.
[11] E. Iglesia, Design, synthesis, and use of cobalt-based Fischer-Tropsch synthesis catalysts, Applied Catalysis A: General, 161 (1997) 59-78.
[12] P.J. vanBerge, R.C. Everson, Natural Gas Conversion IV, 107 (1997) 207-212.
[13] D.I. Enache, B. Rebours, M. Roy-Auberger, R. Revel, In Situ XRD Study of the Influence of Thermal Treatment on the Characteristics and the Catalytic Properties of Cobalt-Based Fischer–Tropsch Catalysts, Journal of Catalysis, 205 (2002) 346-353.
[14] Z. Pan, M. Parvari, D.B. Bukur, Fischer–Tropsch synthesis on Co/ZnO – Two step activation procedure for improved performance, Applied Catalysis A: General, 480 (2014) 79-85.
[15] X.Q. Zhao, S. Veintemillas-Verdaguer, O. Bomati-Miguel, M.P. Morales, H.B. Xu, Thermal history dependence of the crystal structure of Co fine particles, Physical Review B, 71 (2005) 024106.
[16] Y. Choong-Shik, S. Per, C. Hyunchae, The phase diagram of cobalt at high pressure and temperature: the stability of gamma(fcc)-cobalt and new epsilon'(dhcp) -cobalt, Journal of Physics: Condensed Matter, 10 (1998) L311.
[17] V.A. de la Peña O'Shea, P.R. de la Piscina, N. Homs, G. Aromí, J.L.G. Fierro, Development of Hexagonal Closed-Packed Cobalt Nanoparticles Stable at High Temperature, Chemistry of Materials, 21 (2009) 5637-5643.
[18] P. Serna, L.A. Baumes, M. Moliner, A. Corma, Combining high-throughput experimentation, advanced data modeling and fundamental knowledge to develop catalysts for the epoxidation of large olefins and fatty esters, Journal of Catalysis, 258 (2008) 25-34.
[19] U. Rodemerck, D. Wolf, O.V. Buyevskaya, P. Claus, S. Senkan, M. Baerns, High-throughput synthesis and screening of catalytic materials: Case study on the search for a low-temperature catalyst for the oxidation of low-concentration propane, Chemical Engineering Journal, 82 (2001) 3-11.
[20] M. Lucas, P. Claus, High throughput screening in monolith reactors for total oxidation reactions, Applied Catalysis A: General, 254 (2003) 35-43.
[21] H.W. Turner, A.F. Volpe, W.H. Weinberg, High-throughput heterogeneous catalyst research, Surface Science, 603 (2009) 1763-1769.
[22] S. Lögdberg, D. Tristantini, Ø. Borg, L. Ilver, B. Gevert, S. Järås, E.A. Blekkan, A. Holmen, Hydrocarbon production via Fischer–Tropsch synthesis from H2-poor syngas over different Fe-Co/γ-Al_2O_3 bimetallic catalysts, Applied Catalysis B: Environmental, 89 (2009) 167-182.
[23] H. Karaca, O.V. Safonova, S. Chambrey, P. Fongarland, P. Roussel, A. Griboval-Constant, M. Lacroix, A.Y. Khodakov, Structure and catalytic performance of Pt-promoted alumina-supported cobalt catalysts under realistic conditions of Fischer–Tropsch synthesis, Journal of Catalysis, 277 (2011) 14-26.
[24] K. Shimura, T. Miyazawa, T. Hanaoka, S. Hirata, Fischer–Tropsch synthesis over alumina supported cobalt catalyst: Effect of promoter addition, Applied Catalysis A: General, 494 (2015) 1-11.
[25] G. Jacobs, P.M. Patterson, Y. Zhang, T. Das, J. Li, B.H. Davis, Fischer–Tropsch synthesis: deactivation of noble metal-promoted Co/Al_2O_3 catalysts, Applied Catalysis A: General, 233 (2002) 215-226.

[26] Ø. Borg, P.D.C. Dietzel, A.I. Spjelkavik, E.Z. Tveten, J.C. Walmsley, S. Diplas, S. Eri, A. Holmen, E. Rytter, Fischer–Tropsch synthesis: Cobalt particle size and support effects on intrinsic activity and product distribution, Journal of Catalysis, 259 (2008) 161-164.
[27] S. Karimi, A. Tavasoli, Y. Mortazavi, A. Karimi, Cobalt supported on Graphene – A promising novel Fischer–Tropsch synthesis catalyst, Applied Catalysis A: General, 499 (2015) 188-196.
[28] G. Jacobs, T.K. Das, Y. Zhang, J. Li, G. Racoillet, B.H. Davis, Fischer–Tropsch synthesis: support, loading, and promoter effects on the reducibility of cobalt catalysts, Applied Catalysis A: General, 233 (2002) 263-281.
[29] Z. Cai, J. Li, K. Liew, J. Hu, Effect of La_2O_3-dopping on the Al_2O_3 supported cobalt catalyst for Fischer-Tropsch synthesis, Journal of Molecular Catalysis A: Chemical, 330 (2010) 10-17.
[30] S.A. Chernyak, E.V. Suslova, A.V. Egorov, L. Lu, S.V. Savilov, V.V. Lunin, New hybrid CNT–alumina supports for Co-based Fischer–Tropsch catalysts, Fuel Processing Technology, 140 (2015) 267-275.
[31] T.O. Eschemann, J. Oenema, K.P. de Jong, Effects of noble metal promotion for Co/TiO_2 Fischer-Tropsch catalysts, Catalysis Today, 261 (2016) 60-66.
[32] H. Wu, Y. Yang, H. Suo, M. Qing, L. Yan, B. Wu, J. Xu, H. Xiang, Y. Li, Effects of ZrO_2 promoter on physic-chemical properties and activity of $Co/TiO_2–SiO_2$ Fischer–Tropsch catalysts, Journal of Molecular Catalysis A: Chemical, 396 (2015) 108-119.
[33] S.L. Soled, E. Iglesia, R.A. Fiato, J.E. Baumgartner, H. Vroman, S. Miseo, Control of Metal Dispersion and Structure by Changes in the Solid-State Chemistry of Supported Cobalt Fischer–Tropsch Catalysts, Topics in Catalysis, 26 (2003) 101-109.
[34] C.H. Mauldin, S.M. Davis, K.B. Arcuri, Cobalt catalysts for the conversion of methanol and for Fischer-Tropsch synthesis to produce hydrocarbons, in, Google Patents, 1987.
[35] T.E. Feltes, L. Espinosa-Alonso, E.d. Smit, L. D'Souza, R.J. Meyer, B.M. Weckhuysen, J.R. Regalbuto, Selective adsorption of manganese onto cobalt for optimized $Mn/Co/TiO_2$ Fischer–Tropsch catalysts, Journal of Catalysis, 270 (2010) 95-102.
[36] J.A. Delgado, C. Claver, S. Castillón, D. Curulla-Ferré, V.V. Ordomsky, C. Godard, Fischer–Tropsch synthesis catalysed by small TiO_2 supported cobalt nanoparticles prepared by sodium borohydride reduction, Applied Catalysis A: General, 513 (2016) 39-46.
[37] Y. Zhang, K. Liew, J. Li, X. Zhan, Fischer–Tropsch Synthesis on Lanthanum Promoted Co/TiO_2 Catalysts, Catalysis Letters, 139 (2010) 1-6.
[38] A. Juan, D.E. Damiani, Characterization of RuMo-SiO2 catalysts. A comparative study before and after CO hydrogenation reaction, Journal of Materials Chemistry, 6 (1996) 1433-1439.
[39] D. Kistamurthy, A.M. Saib, D.J. Moodley, J.W. Niemantsverdriet, C.J. Weststrate, Ostwald ripening on a planar Co/SiO_2 catalyst exposed to model Fischer–Tropsch synthesis conditions, Journal of Catalysis, 328 (2015) 123-129.
[40] T. Riedel, M. Claeys, H. Schulz, G. Schaub, S.-S. Nam, K.-W. Jun, M.-J. Choi, G. Kishan, K.-W. Lee, Comparative study of Fischer–Tropsch synthesis with H_2/CO and H_2/CO_2 syngas using Fe- and Co-based catalysts, Applied Catalysis A: General, 186 (1999) 201-213.
[41] A.Y. Khodakov, R. Bechara, A. Griboval-Constant, Fischer–Tropsch synthesis over silica supported cobalt catalysts: mesoporous structure versus cobalt surface density, Applied Catalysis A: General, 254 (2003) 273-288.
[42] G.J. Haddad, B. Chen, J.J.G. Goodwin, Effect of La^{3+}Promotion of Co/SiO_2 on CO Hydrogenation, Journal of Catalysis, 161 (1996) 274-281.
[43] A.Y. Khodakov, J. Lynch, D. Bazin, B. Rebours, N. Zanier, B. Moisson, P. Chaumette, Reducibility of Cobalt Species in Silica-Supported Fischer–Tropsch Catalysts, Journal of Catalysis, 168 (1997) 16-25.
[44] A. Michiaki, Y. Kiyotaka, H.Y. Zhuo, F. Kaoru, Fischer–Tropsch Synthesis with Supported Cobalt Catalyst. Promoting Effects of Lanthanum Oxide for Cobalt/Silica Catalyst, Bulletin of the Chemical Society of Japan, 69 (1996) 1509-1516.
[45] M.K. Gnanamani, G. Jacobs, U.M. Graham, M.C. Ribeiro, F.B. Noronha, W.D. Shafer, B.H. Davis, Influence of carbide formation on oxygenates selectivity during Fischer-Tropsch synthesis over Ce-containing Co catalysts, Catalysis Today, 261 (2016) 40-47.
[46] G. Jiao, Y. Ding, H. Zhu, X. Li, J. Li, R. Lin, W. Dong, L. Gong, Y. Pei, Y. Lu, Effect of La_2O_3 doping on syntheses of C1–C18 mixed linear α-alcohols from syngas over the Co/AC catalysts, Applied Catalysis A: General, 364 (2009) 137-142.
[47] J.A. Díaz, A. Romero, A.M. García-Minguillán, A. Giroir-Fendler, J.L. Valverde, Carbon nanofibers and nanospheres-supported bimetallic (Co and Fe) catalysts for the Fischer–Tropsch synthesis, Fuel Processing Technology, 138 (2015) 455-462.
[48] M. Lacroix, L. Dreibine, B. de Tymowski, F. Vigneron, D. Edouard, D. Bégin, P. Nguyen, C. Pham, S. Savin-Poncet, F. Luck, M.-J. Ledoux, C. Pham-Huu, Silicon carbide foam composite containing cobalt as a highly selective and re-usable Fischer–Tropsch synthesis catalyst, Applied Catalysis A: General, 397 (2011) 62-72.

[49] I.G. Solomonik, K.O. Gryaznov, V.F. Skok, V.Z. Mordkovich, Formation of surface cobalt structures in SiC-supported Fischer-Tropsch catalysts, RSC Advances, 5 (2015) 78586-78597.
[50] G.R. Johnson, S. Werner, K.C. Bustillo, P. Ercius, C. Kisielowski, A.T. Bell, Investigations of element spatial correlation in Mn-promoted Co-based Fischer–Tropsch synthesis catalysts, Journal of Catalysis, 328 (2015) 111-122.
[51] M.J. Keyser, R.C. Everson, R.L. Espinoza, Fischer–Tropsch studies with cobalt–manganese oxide catalysts: Synthesis performance in a fixed bed reactor, Applied Catalysis A: General, 171 (1998) 99-107.
[52] S. Zeng, Y. Du, H. Su, Y. Zhang, Promotion effect of single or mixed rare earths on cobalt-based catalysts for Fischer–Tropsch synthesis, Catalysis Communications, 13 (2011) 6-9.
[53] D. Lorito, C. Ruocco, V. Palma, A. Giroir-Fendler, F.C. Meunier, Reconstruction of ceria-supported Pt-Co particles under H_2 and CO at 220°C, Applied Catalysis B: Environmental, 197 (2016) 56-61.
[54] W. Ma, G. Jacobs, T.K. Das, C.M. Masuku, J. Kang, V.R.R. Pendyala, B.H. Davis, J.L.S. Klettlinger, C.H. Yen, Fischer–Tropsch Synthesis: Kinetics and Water Effect on Methane Formation over 25%Co/γ-Al_2O_3 Catalyst, Industrial & Engineering Chemistry Research, 53 (2014) 2157-2166.